Probing High Momentum Protons and Neutrons in Asymmetric Nuclei

M. Duer,[1] O. Hen,[2] Eli Piasetzky,[1] H. Hakobyan,[3] L.B. Weinstein,[4] M. Braverman,[1] E. Cohen,[1] D. Higinbotham,[5] K.P. Adhikari,[29] S. Adhikari,[15] M.J. Amaryan,[4] J. Ball,[10] I. Balossino,[20] L. Barion,[20] M. Battaglieri,[22] V. Batourine,[5,28] I. Bedlinskiy,[26] A.S. Biselli,[13,8] S. Boiarinov,[5] W.J. Briscoe,[18] W.K. Brooks,[3,5] V.D. Burkert,[5] D.S. Carman,[5] A. Celentano,[22] G. Charles,[4] T. Chetry,[32] G. Ciullo,[20,14] L. Clark,[40] Brandon A. Clary,[12] P.L. Cole,[19,9,5] M. Contalbrigo,[20] O. Cortes,[19] V. Crede,[16] A. D'Angelo,[23,35] N. Dashyan,[43] R. De Vita,[22] E. De Sanctis,[21] M. Defurne,[10] A. Deur,[5] C. Djalali,[37] R. Dupre,[25] H. Egiyan,[5] A. El Alaoui,[3] L. El Fassi,[29] P. Eugenio,[16] R. Fersch,[11,42] A. Filippi,[24] T.A. Forest,[19] G. Gavalian,[5,30] Y. Ghandilyan,[43] G.P. Gilfoyle,[34] K.L. Giovanetti,[27] F.X. Girod,[5] E. Golovatch,[36] R.W. Gothe,[37] K.A. Griffioen,[42] L. Guo,[15,5] H. Hakobyan,[3,43] N. Harrison,[5] M. Hattawy,[6] K. Hicks,[32] M. Holtrop,[30] Y. Ilieva,[37,18] D.G. Ireland,[40] B.S. Ishkhanov,[36] E.L. Isupov,[36] K. Joo,[12] M.L. Kabir,[29] D. Keller,[41] G. Khachatryan,[43] M. Khachatryan,[4] M. Khandaker,[31,*] A. Kim,[12] W. Kim,[28] A. Klein,[4] F.J. Klein,[9] S.E. Kuhn,[4] L. Lanza,[23] P. Lenisa,[20] K. Livingston,[40] I .J .D. MacGregor,[40] N. Markov,[12] B. McKinnon,[40] V. Mokeev,[5,36] R.A. Montgomery,[40] A Movsisyan,[20] C. Munoz Camacho,[25] P. Nadel-Turonski,[5] S. Niccolai,[25] G. Niculescu,[27] M. Osipenko,[22] A.I. Ostrovidov,[16] M. Paolone,[38] K. Park,[5,28] David Payette,[4] W. Phelps,[15] O. Pogorelko,[26] J. Poudel,[4] J.W. Price,[7] S. Procureur,[10] Y. Prok,[4,41] D. Protopopescu,[40] A. Rizzo,[23,35] G. Rosner,[40] P. Rossi,[5,21] F. Sabatié,[10] C. Salgado,[31] R.A. Schumacher,[8] Y.G. Sharabian,[5] G.D. Smith,[39] N. Sparveris,[38] S. Stepanyan,[5] S. Strauch,[37,18] M. Taiuti,[17,†] J.A. Tan,[28] M. Ungaro,[5,33] H. Voskanyan,[43] E. Voutier,[25] D.P. Watts,[39] X. Wei,[5] N. Zachariou,[39] J. Zhang,[41] and Z.W. Zhao[4]

(The CLAS Collaboration)

[1] *Tel Aviv University, Tel Aviv, Israel*

[2] *Massachusetts Institute of Technology, Cambridge, MA, 02139*

[3] *Universidad Técnica Federico Santa María, Casilla 110-V Valparaíso, Chile*

[4] *Old Dominion University, Norfolk, Virginia 23529*

[5]*Thomas Jefferson National Accelerator Facility, Newport News, Virginia 23606*
[6]*Argonne National Laboratory, Argonne, Illinois 60439*
[7]*California State University, Dominguez Hills, Carson, CA 90747*
[8]*Carnegie Mellon University, Pittsburgh, Pennsylvania 15213*
[9]*Catholic University of America, Washington, D.C. 20064*
[10]*IRFU, CEA, Universit'e Paris-Saclay, F-91191 Gif-sur-Yvette, France*
[11]*Christopher Newport University, Newport News, Virginia 23606*
[12]*University of Connecticut, Storrs, Connecticut 06269*
[13]*Fairfield University, Fairfield CT 06824*
[14]*Universita' di Ferrara , 44121 Ferrara, Italy*
[15]*Florida International University, Miami, Florida 33199*
[16]*Florida State University, Tallahassee, Florida 32306*
[17]*Università di Genova, 16146 Genova, Italy*
[18]*The George Washington University, Washington, DC 20052*
[19]*Idaho State University, Pocatello, Idaho 83209*
[20]*INFN, Sezione di Ferrara, 44100 Ferrara, Italy*
[21]*INFN, Laboratori Nazionali di Frascati, 00044 Frascati, Italy*
[22]*INFN, Sezione di Genova, 16146 Genova, Italy*
[23]*INFN, Sezione di Roma Tor Vergata, 00133 Rome, Italy*
[24]*INFN, Sezione di Torino, 10125 Torino, Italy*
[25]*Institut de Physique Nucléaire, CNRS/IN2P3 and Université Paris Sud, Orsay, France*
[26]*Institute of Theoretical and Experimental Physics, Moscow, 117259, Russia*
[27]*James Madison University, Harrisonburg, Virginia 22807*
[28]*Kyungpook National University, Daegu 41566, Republic of Korea*
[29]*Mississippi State University, Mississippi State, MS 39762-5167*
[30]*University of New Hampshire, Durham, New Hampshire 03824-3568*
[31]*Norfolk State University, Norfolk, Virginia 23504*
[32]*Ohio University, Athens, Ohio 45701*
[33]*Rensselaer Polytechnic Institute, Troy, New York 12180-3590*
[34]*University of Richmond, Richmond, Virginia 23173*
[35]*Universita' di Roma Tor Vergata, 00133 Rome Italy*

[36]*Skobeltsyn Institute of Nuclear Physics, Lomonosov Moscow State University, 119234 Moscow, Russia*
[37]*University of South Carolina, Columbia, South Carolina 29208*
[38]*Temple University, Philadelphia, PA 19122*
[39]*Edinburgh University, Edinburgh EH9 3JZ, United Kingdom*
[40]*University of Glasgow, Glasgow G12 8QQ, United Kingdom*
[41]*University of Virginia, Charlottesville, Virginia 22901*
[42]*College of William and Mary, Williamsburg, Virginia 23187-8795*
[43]*Yerevan Physics Institute, 375036 Yerevan, Armenia*

(Dated: December 12, 2017)

Abstract

Abstract here

PACS numbers:

* Current address:Idaho State University, Pocatello, Idaho 83209

† Current address:INFN, Sezione di Genova, 16146 Genova, Italy

Probing High Momentum Protons and Neutrons in Asymmetric Nuclei

M. Duer, O. Hen, Eli Piasetzky, H. Hakobyan, L.B. Weinstein, M. Braverman, E. Cohen, D. Higinbotham et al.
(CLAS Collaboration)

The atomic nucleus is one of the densest and most complex quantum-mechanical systems in nature. Nuclei account for nearly all the mass of the visible universe. The properties of individual protons and neutrons (nucleons) in nuclei can be studied by scattering a high-energy particle from the nucleus and detecting this particle after it scatters, often also detecting an additional knocked-out proton. Electron scattering experiments demonstrate that about 20% of the nucleons in nuclei have momentum greater than the nuclear Fermi momentum, k_F, and that this 'high-momentum tail' is predominantly due to close-proximity neutron-proton (np) pairs that interact via a strong short-range force [1-11]. These np pairs were measured directly in electron scattering experiments from helium-4 and carbon [2, 4-6], but only inferred in heavier nuclei [3]. We measured protons and, for the first time, neutrons knocked out of medium to heavy nuclei by high-energy electrons. We found that the fraction of high-momentum protons increases dramatically with the neutron excess, while the fraction of high-momentum neutrons decreases slightly. This indicates that protons move faster than neutrons in neutron-rich nuclei, an effect that we call momentum-sharing inversion. This effect is surprising, since in the nuclear shell model protons and neutrons obey Fermi statistics and independently fill energy shells. Modern calculations also omit the momentum-sharing inversion when they truncate the contributions of high-momentum nucleons [12]. These approximations work well for describing gross, low-energy properties of nuclei. However, we need to understand the nature of the high-momentum distribution in asymmetric nuclei to study systems such as neutron stars [13, 14] and the modification of the internal structure of nucleons bound in nuclei [1, 15-16]. In particular, the neutron excess in neutron stars should dramatically increase the average momentum of the protons, which could have significant implications for their cooling rate and equation of state.

Since the 1950s, the nuclear shell model has been an indispensable guide for understanding nuclei [17]. In this model, nucleons move independently in well-defined quantum orbits (shells) similarly to electrons in atoms. The potential in which the nucleons move is the average nuclear field created by their strong mutual interactions. While successful in making many important predictions, this textbook picture of the nucleus is quite incomplete: electron scattering experiments in nuclei ranging from lithium to lead measured only about 60%–70% of the expected number of protons in each shell [18].

Modern superconducting accelerators, with high-energy, high-intensity, and high-duty-factor, allow experiments that use scattering reactions to resolve the structure and dynamics of individual nucleons and nucleon pairs in nuclei. These experiments have shown that about 20% of the nucleons in nuclei do not occupy a shell-model state; they are instead coupled into short-lived correlated nucleon-pairs with large relative momentum ($k_{relative} > k_F$) and small center-of-mass (CM) momentum ($k_{CM} < k_F$), referred to as short-range correlated (SRC) pairs [1-11]. These pairs are entirely absent in the shell model description of nuclei.

The dominant force between the nucleons in the SRC pairs is tensor in nature [1]. This pair-wise interaction acts predominantly on spin-1 np-SRC pairs, leading to a predominance of np-SRC pairs over proton-proton (pp) and neutron-neutron (nn) SRC pairs by a factor of about 20. This phenomenon is referred to as "np-dominance" [2-7].

Almost all high-momentum nucleons in nuclei belong to an SRC pair. As the short-distance interaction between nucleons in SRC pairs is very strong, the characteristics of the resulting pairs are largely independent of the rest of the nucleus. Thus the high-momentum tail has a universal shape for all nuclei [1, 8-11, 19].

According to the shell model, adding neutrons to a nucleus increases the average neutron momentum without significantly affecting the average proton momentum. However, if correlations are included, adding neutrons could increase the number of np SRC pairs and hence the number of high-momentum protons [3, 20-21].

The analysis reported here was motivated by the quest to directly observe and quantify the relative number of protons and neutrons in the high momentum tails of neutron-rich nuclei [20]. For the first time, we simultaneously measured electron-induced quasi-elastic (QE) knockout of protons and neutrons from medium and heavy nuclei, using the A(e,e'p) and A(e,e'n) reactions, respectively. The simultaneous measurement of both proton and neutron knockout is the unique feature of this work that allows us to directly compare their properties using minimal assumptions. Data from these measurements perform four functions: (1) quantifying the relative fractions of high-momentum protons and neutrons, (2) showing that adding *neutrons* to the nucleus increases the fraction of high-momentum *protons*, (3) helping confirm the np-SRC dominance of the high-momentum tail in medium and heavy nuclei, and (4) supporting momentum-sharing inversion in heavy nuclei.

The data presented here were collected in 2004 in Hall-B of the Thomas Jefferson National Accelerator Facility (Jefferson Lab) in Virginia, USA to study various reactions [22-23]. The experiment used a 5.014 GeV electron beam incident on deuterium, carbon, aluminum, iron, and lead targets, and the CEBAF Large Acceptance Spectrometer (CLAS) [24] to detect the scattered electron

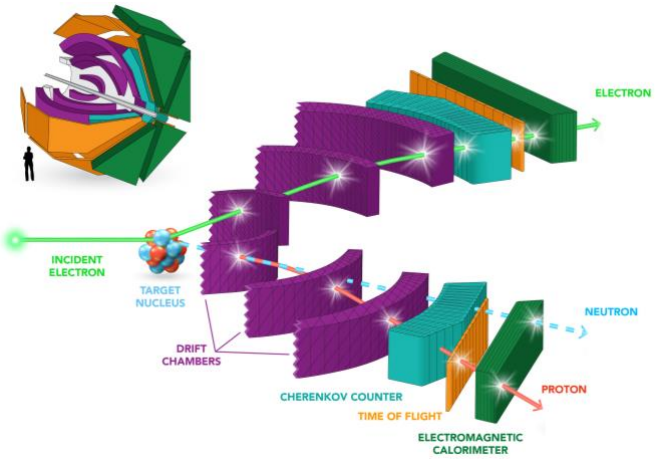

Fig 1 | The CLAS Spectrometer. Inset: the almost spherical CLAS. The electron beam travels along the gray pipe, hitting a target near the center of the spectrometer. Main image: Two segments of CLAS. Electrons traveling with energies up to 6 billion electron volts hit nuclei, knocking out individual protons and neutrons. The momenta of the scattered electrons and knocked-out protons are reconstructed by analyzing their trajectories as they bend in a toroidal magnetic field. The neutron momenta are deduced from their time of flight until they interact with the electromagnetic calorimeter.

and any associated hadrons knocked out during the interaction (see Fig. 1). CLAS used a toroidal magnetic field and six independent sets of drift chambers, time-of-flight scintillation counters, Cherenkov counters, and electromagnetic calorimeters, covering scattering angles from about 8° to 140° for charged-particle identification and trajectory reconstruction. The neutrons were identified by observing interactions in the forward electromagnetic calorimeters (covering about 8° to 45°) with no associated charged-particle tracks in the drift chambers. The angle- and momentum-dependent neutron detection efficiency and momentum reconstruction resolution were measured simultaneously using the $d(e,e'p\pi^+\pi^-n)$ reaction [25]. The experiment recorded all events with a scattered electron detected in both the electromagnetic calorimeter and the Cherenkov counter, along with any other particles. This feature allowed us to re-analyze the data as part of the Jefferson Lab data-mining initiative to study a wide range of new phenomena not considered in the original experimental proposals [3, 26-27].

High-energy electrons scatter from the nucleus by transferring a single virtual photon, carrying momentum $\vec{q}$ and energy ω. In QE scattering, this momentum transfer is absorbed by a nucleon with initial momentum $\vec{p}_i$. If the nucleon does not rescatter as it leaves the nucleus, then it will emerge with momentum $\vec{p}_N = \vec{p}_i + \vec{q}$. Thus, we can reconstruct the approximate initial momentum of the nucleon from the missing momentum, the difference between the detected nucleon momentum and the transferred momentum: $\vec{p}_{miss} = \vec{p}_N - \vec{q}$. Similarly, the excitation energy of the residual (A-1) nucleus is related to the missing energy, $E_{\rm miss} = \omega - T_N$, where T_N is the nucleon's kinetic energy.

In this analysis, we studied (e,e'p) and (e,e'n) QE knockout event samples measured in two kinematical regions, corresponding to electron scattering off high-initial-momentum ($p_i > k_F$) nucleons, presumably from an SRC pair, or from low-initial-momentum ($p_i < k_F$) nucleons, presumably from shell model states.

Using these event samples, we derived both the ratio of A(e,e'n)/A(e,e'p) events for each setting and the double ratio of high-momentum (SRC) to low-momentum (shell-model) nucleons in nuclei relative to carbon, $[A(e,e'N)_{High} / A(e,e'N)_{Low}] / [^{12}C(e,e'N)_{High} / ^{12}C(e,e'N)_{Low}]$. Here N refers to either protons or neutrons, and A stands for either aluminum, iron, or lead. The double-ratio is simply an estimator for the increased fraction of SRC nucleons in an asymmetric nucleus compared to carbon. We use carbon as a reference since it is a well-studied, medium-mass, symmetric nucleus and has similar average density to the other measured nuclei. In addition, forming cross-section ratios relative to carbon also significantly reduces the effects of detector acceptance and efficiency corrections [25].

For each kinematical setting, we used the same selection criteria on the detected scattered electron and associated knocked-out nucleon (proton or neutron) to select QE A(e,e'p) and A(e,e'n) events. The extraction of equivalent (e,e'p) and (e,e'n) event samples required determining the common angular region for detecting both protons and neutrons, correcting for the neutron and proton detection efficiencies, and accounting for the different momentum resolutions. The latter was a significant challenge as, being neutral particles, neutrons do not interact in the tracking system. Thus, their momentum must be inferred from the time difference between the electron scattering in the target and the neutron detection in the calorimeter, leading to about 10 - 15% momentum resolution for the detected neutrons [25]. Proton momenta were determined to an uncertainty of about 1% from the curvature of their trajectories in the CLAS magnetic field.

We accounted for this momentum resolution difference by: (1) selecting the desired A(e,e'p) events in high- and low-momentum kinematics, (2) "smearing" the proton momentum for each event using the measured neutron momentum resolution, and (3) using unsmeared and smeared A(e,e'p) event samples to study bin migration effects and optimize the event selection criteria. This allowed us to produce a smeared event sample with as many of the 'original' A(e,e'p) events as possible (i.e. high selection efficiency), and as few other events as possible (i.e. high purity). We used the smeared proton momenta in the final selection of A(e,e'p) events for consistency with the A(e,e'n) analysis. The final event selection criteria are detailed below.

Low-initial-momentum events are characterized by low missing energy and low missing momentum ($E_{miss} < 80$-90 MeV; and $p_{miss} = |\vec{p}_{miss}| < 250$ MeV/c) [25]. Because the neutron resolution was not good enough to select these events directly, we developed a set of alternative constraints to select the same events by using

the detected electron momentum and the knocked-out nucleon angle, which were unaffected by the neutron momentum resolution [25]. We optimized these constraints using the unsmeared and smeared protons so that the final event sample contains about 90% of the desired sample with about 15% contamination, resulting in about 5% more events in our sample. We assumed cross section corrections of about 5%, which caused a less than 1% correction to ratios between different nuclei. We assumed systematic uncertainties equal to the corrections, see Supplementary Material for details.

Similarly, we selected the high-initial-momentum events in two steps. We first selected QE events with a leading nucleon by cutting on the energy and momentum transfer and requiring that the outgoing nucleon be emitted with most of the transferred momentum in the general direction of the momentum transfer. We then selected high-initial-momentum events by requiring large missing momentum ($p_{miss} > 300$ MeV/c). These selection criteria ensured that the electron interacted with a single high-initial-momentum proton or neutron in the nucleus [3, 27]. We then optimized the nucleon-momentum dependent cuts using the smeared and unsmeared protons. This gave us a final event sample with 85% of the desired sample and about 15% contamination, resulting in about the same number of events. We corrected for this when extracting the cross-section ratios. The procedures for the extraction of cross-section ratios and their associated systematic uncertainties from the measured event yields are detailed in the supplementary materials [25].

To verify the neutron detection efficiency, detector acceptance corrections, and event selection method, we extracted the carbon neutron-to-proton reduced cross-section ratio for both high and low initial nucleon momenta: [^{12}C(e,e'n)/ σ_n] / [^{12}C(e,e'p)/σ_p] (i.e. measured cross-sections scaled by the known elastic electron-proton σ_p and electron-neutron σ_n cross-sections). Figure 2 shows these two measured cross-section ratios are consistent with unity, as expected for a symmetric nucleus. This shows that in both high- and low-initial-momentum kinematics we have restricted the reaction mechanisms to primarily QE scattering and have correctly accounted for the various detector-related effects.

For the other measured nuclei, the (e,e'n)/(e,e'p) low-momentum reduced cross-section ratios grow approximately as N/Z, as expected from simple nucleon counting. However, the (e,e'n)/(e,e'p) high-momentum ratios are consistent with unity for all measured nuclei, see Fig. 2.

The struck nucleons could reinteract as they emerged from the nucleus. Such an effect would cause the number of detected outgoing nucleons to decrease and modify the angles and momenta of the knocked-out nucleons. The decrease in the measured cross section would be nearly identical for protons and neutrons and thus, any effects should cancel when forming cross-section ratios [25]. Since rescattering changes the event kinematics, some of the events with high measured p_{miss} could have originated from electron scattering from a low-initial-momentum nucleon, which then rescattered, increasing p_{miss}. If the high-initial-momentum (high-p_{miss}) nucleons were caused by electron scattering from the more-numerous low-initial-momentum nucleons followed by nucleon rescattering, then the high-momentum (e,e'n)/(e,e'p) ratio would show the same N/Z dependence as the low-momentum ratio. As the high-momentum (e,e'n)/(e,e'p) ratio is independent of A, nucleon-rescattering effects must be small.

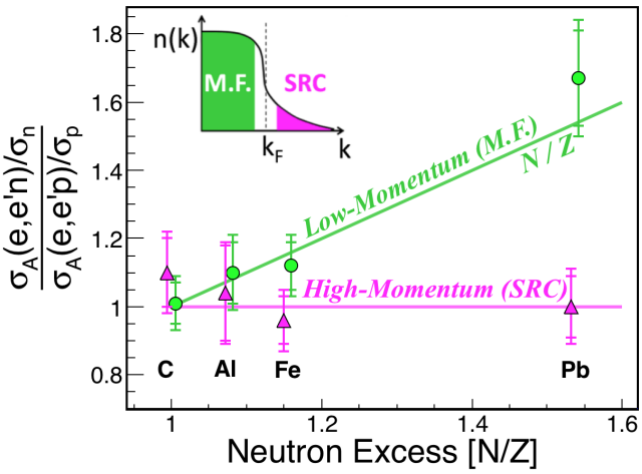

Fig 2 | The relative abundances of high- and low-initial-momentum neutrons and protons. [A(e,e'n)/ σ_n] / [A(e,e'p)/σ_p] reduced cross-section ratio for low-momentum (green circles) and high-momentum (purple triangles) events. The initial nucleon momenta corresponding to each type of event are illustrated in the inset. The lines show the simple N/Z expectation for low-momentum nucleons and the np-dominance expectation (i.e., ratio = 1) for high-momentum nucleons. The inner error bars are statistical while the outer ones include both statistical and systematic uncertainties [25].

Thus, these data indicate that there are equal numbers of high-initial-momentum protons and neutrons in asymmetric nuclei, even though these nuclei contain up to 50% more neutrons than protons. This observation is consistent with high-momentum nucleons belonging primarily to np-SRC pairs, even in neutron rich nuclei [20]. This number equality implies a greater fraction of high-initial-momentum protons. For example, if 20% [1] of the 208 nucleons in lead-208 are at high-initial-momentum, then these consist of 21 protons and 21 neutrons. This corresponds to a high-momentum proton fraction of 21/82 ~ 25% and a corresponding neutron fraction of only 21/126 ~ 17%.

In order to quantify the relative fraction of high-momentum protons and neutrons in the different nuclei with minimal experimental and theoretical uncertainties, we extracted the double ratio of (e,e'N) high-initial-momentum to low-initial-momentum events for nucleus A relative to carbon for both protons and neutrons. We find that the fraction of high-initial-momentum protons *increases* by about 50% from carbon to lead (see Fig. 3).

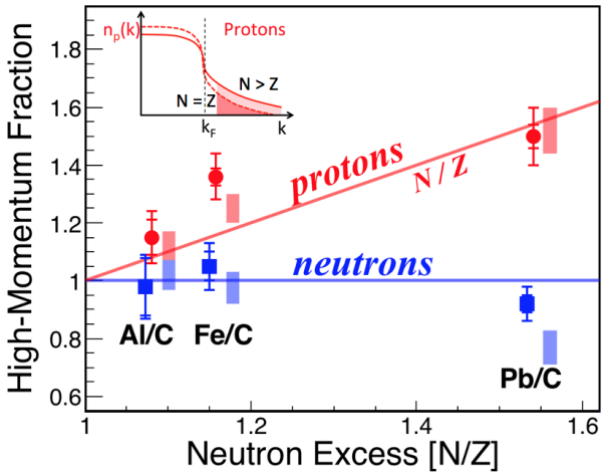

Fig 3 | Relative high-momentum fractions for neutrons and protons. Red circles: The double ratio of the number of (e,e'p) high-momentum proton events to low-momentum proton events for nucleus A relative to carbon. The inner error bars are statistical while the outer ones include both statistical and systematic uncertainties. Red bands: the prediction of the phenomenological np-dominance model [25]. Blue squares and bands: the same for neutron events. The inset demonstrates how adding neutrons increases the fraction of protons in the high momentum tail. The red line at *N*/*Z* and the blue line at 1 are drawn to guide the eye.

Moreover, the corresponding fraction of high-initial-momentum neutrons seems to *decrease* by about 10%. Nucleon-rescattering should increase in larger nuclei and should affect protons and neutrons equally. Since, unlike the protons, the neutron ratio decreases with A, this also rules out significant nucleon rescattering effects.

To determine whether the observed high-initial-momentum proton fraction is large enough to make the average kinetic energy of protons larger than that of neutrons in heavy neutron-rich nuclei, we compared it to a simple phenomenological (i.e. experiment-based) np-dominance model [3, 20] that uses the mean-field momentum distributions from one of three different models at low momentum ($k < k_F$) and a deuteron-like high-momentum tail, scaled by the measured fraction of high-momentum nucleons in nuclei [25]. The model predictions for the relative fractions of high-momentum nucleons agree with the data, increasing our confidence in the model, see Fig. 3. This model also predicts a neutron-to-proton average kinetic energy ratio ($<E^{kin}_n>/<E^{kin}_p>$) that decreases with neutron excess, reaching 0.8 for lead [3, 20-21, 25]. The data therefore present a first direct experimental indication that on average protons move faster than neutrons in neutron-rich nuclei.

The surprising fact that increasing the number of *neutrons* in a nucleus increases the fraction of high-initial-momentum *protons*, predicted by [20] and calculated by [3, 21], has several broad implications. Neutron stars contain about 5 to 10% protons and electrons in their central layers [28]. Our work implies that the extreme neutron excess in a neutron star would dramatically increase the average momentum of the small minority of protons. This disproportionately large effect could have significant implications for the cooling rate and equation of state of neutron stars [13 ,14] and thus needs to be addressed in realistic descriptions of these systems.

There is evidence that the high-momentum nucleons associated with SRC pairs are responsible for the EMC effect, the change in the quark distribution of nucleons bound in nuclei [1, 15]. The EMC effect may result from temporary high-density fluctuations in the nucleus in which the internal structure of the affected nucleons is briefly modified [1]. If this mechanism indeed occurs, then the higher-momentum minority protons in neutron-rich nuclei should be more modified than the neutrons. Observing such increased modification of the proton structure in neutron rich nuclei could shed new light on the currently unknown origin of these modifications.

Furthermore, the existence of short range correlated pairs in nuclei and their np dominance in heavy nuclei has significant implications in many areas of nuclear physics, including nuclear correlation functions and the double beta decay rate of nuclei [29], the nature of the repulsive core of the nucleon-nucleon interaction [4], and our understanding of neutrino-nucleus interactions [30].

References:

1. O. Hen et al., Rev. Mod. Phys. **89**, 045002 (2017).
2. R. Subedi et al., Science **320**, 1476 (2008).
3. O. Hen et al., Science **346**, 614 (2014).
4. I. Korover, N. Muangma, O. Hen et al., Phys. Rev. Lett. **113**, 022501 (2014).
5. E. Piasetzky et al., Phys. Rev. Lett. **97**, 162504 (2006).
6. A. Tang et al., Phys. Rev. Lett. **90**, 042301 (2003).
7. H. Baghdasaryan et al. (CLAS Collaboration), Phys. Rev. Lett. **105**, 222501 (2010).
8. N. Fomin et al., Phys. Rev. Lett. **108**, 092502 (2012).
9. K. Egiyan et al. (CLAS Collaboration), Phys. Rev. Lett. **96**, 082501 (2006).
10. L.L. Frankfurt et al., Phys. Rev. C **48**, 2451 (1993).
11. J. Arrington et al., Prog. Part. Nucl. Phys. **67**, 898 (2012).
12. E. Epelbaum, H.W. Hammer, and U.G. Meissner, Rev. Mod. Phys. **81**, 1773 (2009).
13. L. Frankfurt, M. Sargsian, and M. Strikman, Int. J. Mod. Phys. A **23**, 2991 (2008).
14. B.J. Cai and B.A. Li, arXiv: 1703.08743 (2017).
15. L.B. Weinstein et al., Phys. Rev. Lett. **106**, 052301 (2011).
16. O. Hen, E. Piasetzky, and L.B. Weinstein, Phys. Rev. C **85**, 047301 (2012).
17. E. Caurier et al., Rev. Mod. Phys. **77**, 427 (2005).
18. J.J. Kelly, Adv. Nucl. Phys. **23**, 75 (1996).
19. L.L. Frankfurt and M.I. Strikman, Phys. Rep. **76**, 215 (1981).
20. M.M. Sargsian, Phys. Rev. C **89**, 034305 (2014).
21. Jan Ryckebusch, Maarten Vanhalst, and Wim Cosyn, J. Phys. G. **42**, 055104 (2015).
22. A. Daniel et al. (CLAS Collaboration), Phys. Lett. B **706**, 26 (2011).

23. L. El Fassi et al., Phys. Lett. B **712**, 326 (2012).
24. B.A. Mecking et al., Nucl. Instrum. Methods A **503** (2003) 512.
25. Online Supplementary Materials.
26. L.B. Weinstein et al., "Short distance structure of nuclei: Mining the wealth of existing Jefferson Lab data," DOE Grant DE-SC0006801.
27. O. Hen et al., Phys. Lett. B **722**, 63 (2013).
28. J. Lattimer and M. Prakash, Science **304**, 536 (2004).
29. M. Kortelainen and J. Suhonen, Phys. Rev. C **76**, 024315 (2007).
30. H. Gallagher, G. Garvey, and G.P. Zeller, Ann. Rev. Nuc. Part. Sci. **61**, 355 (2011).